Perfect THz absorber based on vanadium dioxide

RISHABH AGARWAL, SURENDRA KUMAR GUPTA, AMIT BAGE*
Department of Electronics and Communication Engineering, National Institute of Technology, Hamirpur, Himachal Pradesh, 177005, India

This work proposes a novel metamaterial perfect absorber (MPA) for the terahertz (THz) frequency range. The MPA utilizes a split-ring star-shaped pattern fabricated from vanadium dioxide (VO_2) on a silicon dioxide (SiO_2) dielectric substrate. The CST Microwave Studio is used for structure's absorption performance. The design employs a sub-wavelength unit cell to create a near-infinite periodic array. Numerical analysis of unit cell's shows absorption of 99.79% at a specific frequency of 4.108 THz. Furthermore, the MPA demonstrates a broad terahertz absorption bandwidth exceeding 90% ranging from 3.541 THz to 4.773 THz, which translates to a bandwidth of 1.232 THz.

(Received July 18, 2024; accepted December 2, 2024)

Keywords: Absorber, Metamaterials, Perfect absorption, Silicon dioxide, THz, Vanadium dioxide

1. Introduction

Terahertz wave applications and metamaterials in electromagnetic wave absorbers are two of the main areas of focus for multidisciplinary scientific research being conducted right now. Metamaterials are a novel class of synthetic electromagnetic materials composed of periodic arrays of subwavelength unit structures. Usually composed of basic electric or magnetic resonance units, they can produce resonance effects on electromagnetic waves in particular bands [1]. As such, their application allows for the artificial manipulation of electromagnetic waves to generate particular electromagnetic properties that are not found in nature [2]. Terahertz radiation also contains a wealth of physical and chemical information, and the photons in it have low energies and do not damage matter. There has been a lot of interest in research because of the many benefits of terahertz waves [3]. The wide bandwidth, high permeability, and other advantageous characteristics of terahertz waves make them ideal for high-definition imaging and broadband communications. Numerous functional devices, including absorbers [4], filters [5], polarization converters [6], and many more, based on various metamaterials have been proposed to advance the development of terahertz technology.

Terahertz technology holds immense potential in various applications, including energy harvesting [7], reducing unwanted scattering [8], and thermal sensing [9]. Metamaterial perfect absorbers (MPAs) play a crucial role in these advancements. By carefully manipulating electric and magnetic resonances to exploit beneficial material losses, metamaterials can achieve near-perfect absorption. However, the initial designs of metamaterial absorbers suffered from limitations, they had narrow bandwidths and were sensitive to light polarization, hindering their real-world usability [10]. To address these limitations, significant research efforts have focused on broadening the absorption bandwidth of metamaterial absorbers. Initially, a proposal for the MPA in the microwave range is demonstrated in [11]. It is made up of a bottom metal ground plane and a top metal pattern divided by a dielectric layer. Subsequently, the MPA has undergone extensive development, expanding beyond the microwave frequency band to encompass full-spectrum applications in terahertz, infrared, visible light, ultraviolet, and other wavelengths. The aforementioned MPAs have fixed electromagnetic absorption peaks and a narrow absorption bandwidth, though. Their practical application is limited by these imperfections when taking into account a higher THz bandwidth and greater flexibility.

The realization of THz MPAs with broadband absorption capabilities and reconfigurable characteristics has drawn the attention of numerous researchers recently. Multiple resonant structures of varying sizes and multi-layer structures with dielectric layers of varying thicknesses are suggested to achieve broadband absorption [12]. These structures are constrained, though, by their difficult controllability and intricate manufacturing process. Concurrently, several tunable hybrids MPAs based on phase change material, liquid crystal, semiconductor, and graphene have been reported to achieve reconfigurable characteristics [13]. Consequently, it is anticipated that vanadium dioxide (VO_2) will exhibit dynamically adjustable properties in the THz range as an effective metamaterial component. Some VO_2 based MPAs with adjustable absorption characteristics have been introduced recently. The adjustable range and the absorption bandwidth, however, have not yet lived up to the demands of real-world applications.

In this paper, a split-ring star-shaped VO_2 based metamaterial absorber is proposed for the THz applications. Our design utilizes a sub-wavelength unit cell to create a virtually infinite periodic array. This configuration allows for efficient light absorption. To optimize the absorber's performance and reliability, we meticulously analyzed its dimensions through

comprehensive full-wave simulations. These simulations were performed using CST Microwave Studio, a commercially available software that employs the finite-integration technique. The proposed metamaterial absorber achieves an impressive absorption of 99.79% at a specific THz frequency (4.108 THz). Furthermore, it demonstrates a broad THz absorption bandwidth exceeding 90%. This bandwidth ranges from 3.541 THz to 4.773 THz, translating to a remarkable 1.232 THz. The exceptional absorption can be explained by two key theoretical principles: impedance matching theory and interference cancellation theory. These principles offer a physical understanding of how the design effectively absorbs incoming THz radiation. The remaining sections of this paper delve deeper into the design process. Section 2 details the initial design concept, its theoretical description, and the evolution of the absorber and parametric analysis. Section 3 presents the results and a comprehensive discussion. Finally, Section 4 concludes the paper with key takeaways.

2. Absorber design

2.1. Theoretical description of the metamaterial-based absorber

To achieve the most accurate simulations, the materials within the structure are modelled using the Drude model. This model effectively captures the optical properties of VO_2 and gold (*Au*) at THz frequencies, as detailed in [14]. When an electromagnetic (*EM*) wave interacts with the metamaterial surface, it can be either reflected or transmitted. The goal is to minimize both reflectance and transmittance, thereby maximizing absorption. Eq. (1) [15] expresses this concept mathematically, where absorption, $A(\omega)$ is directly related to the sum of reflectance, $R(\omega)$ and transmittance, $T(\omega)$.

$$A(\omega) = 1 - R(\omega) - T(\omega) \tag{1}$$

We can calculate the reflection coefficient under normal incidence using Eq. (2).

$$R(\omega) = \frac{Z(\omega) - Z_0}{Z(\omega) + Z_0} \tag{2}$$

As shown in Eq. (2), the reflection coefficient depends on the impedances of free space (Z_0) and the metamaterial absorber ($Z(\omega)$) [16]. Ideally, for zero reflection to occur, these impedances need to be perfectly matched ($Z_0 = Z(\omega)$). To effectively characterize this metamaterial, we consider its frequency-dependent properties. These properties are described by its relative electric permittivity ($\varepsilon_r(\omega) = \dot{\varepsilon}(\omega) + \ddot{\varepsilon}(\omega)$) and relative permeability ($\mu_r(\omega) = \dot{\mu}(\omega) + \ddot{\mu}(\omega)$) at a specific frequency (ω). Using these values, Eqs. (3) and (4) [15] allow us to calculate the device impedance of the metamaterial absorber.

$$R(\omega) = \sqrt{\frac{\mu_0 \mu_r(\omega)}{\varepsilon_0 \varepsilon_r(\omega)}} \tag{3}$$

$$Z_0 = \sqrt{\frac{\mu_0}{\varepsilon_0}} \tag{4}$$

where ε_0 and μ_0 are the free space permittivity and permeability, respectively.

Perfect absorption hinges on manipulating the metamaterial's properties to match the impedance of free space. This is achieved by tailoring the relative ε_r and μ_0 (as described in Eqs. (3) and (4)) to be indistinguishable from those of free space (Z_0). At this point of impedance matching, the incoming *EM* wave is entirely absorbed by the metamaterial with no reflection. However, achieving perfect absorption requires eliminating transmission as well. A ground plane made of metal, with a thickness exceeding the skin depth at the operating frequency [17], effectively reflects any transmitted wave into the metamaterial, preventing it from escaping. Careful material selection and adjustments to the metamaterial unit cell's geometry can create resonance at the desired frequency. At this resonance point, the transmission term is minimized, further enhancing absorption. Therefore, by controlling these material properties and geometric characteristics, we can minimize the reflection coefficient and achieve near-perfect absorption.

2.2. Unit-cell design

The schematic of the proposed unit cell structure and the perceptive view of the THz MPA are depicted in Figs. 1(a) and (b), respectively. The proposed MPA is made up of three layers: SiO_2 dielectric layer is embedded in a VO_2 pattern (top layer), and an optically thick gold film (bottom layer). As demonstrated prior, the THz dielectric properties of VO_2 in its metallic phase can be effectively modelled using the Drude equation (Eq. (5)).

$$\varepsilon(\omega) = \varepsilon_\infty - \frac{{\omega_P}^2}{(\omega^2 + i\gamma\omega)} \tag{5}$$

where ε_∞ is the permittivity at high frequency, ω_P is the conductivity-dependent plasmon frequency and γ is the collision frequency [18]. Furthermore, the plasmon frequency (ω_P) can be approximated using Eq. (6), which provides a way to estimate this value based on the material's properties.

$$\omega_P(\sigma) = \omega_P(\sigma_0) \times \sqrt{\frac{\sigma}{\sigma_0}} \tag{6}$$

From measured data [19], we have determined that when $\sigma_0 = 2 \times 10^5$ S/m ($\varepsilon_\infty = 12$), it follows that the corresponding $\omega_P(\sigma_0) = 1.4 \times 10^{15}$ rad/s, while $\gamma = 5.75 \times 10^{13}$ rad/s is assumed to be independent of σ. A SiO_2 layer with optimized thickness is sandwiched between the VO_2 and gold layer to further improve the impedance matching condition. Hence, the absorber can be able to fully absorb the incident electromagnetic waves if the SiO_2 is relatively

thick [20]. The relative dielectric constant of the SiO_2 dielectric layer is $\varepsilon = 3.8$, and the thickness of is SiO_2 layer (h) is 9 μm. Enhancing the absorption effect, a bottom gold layer thicker than the terahertz wave's skin depth can stop transmission and reflect the incident electromagnetic wave into the structure [21]. The gold layer has an optimised thickness of the gold film is 0.2 μm and the conductivity of the gold film is 4.56×10^7 S/m.

The top of the proposed absorber having a VO_2 layer is made up of two semicircular rings separated by a distance of $g = 10$ μm and an outer radius of $R = 18.48$ μm to form a split-ring structure. Further to form a star-shaped structure, ten VO_2 strips having length $d = 14$ μm are hinged at their centre with equal angular spacing. Further, utilising the proposed unit absorber a THz MPA based on a doubly periodic array of VO_2 structures is proposed, as depicted in Fig. 2. The combined effect of the VO_2 pattern and the three-layer structure ($VO_2/SiO_2/Au$) is expected to generate multiple overlapping resonances. These resonances are crucial for achieving perfect absorption. Broadband THz waves incident on the structure from the top. For clarity, we can further explain that the magnetic field is oriented along the y-axis, while the electric field is oriented along the x-axis. It's important to note that subsequent analysis focuses on the individual unit cell rather than the entire structure.

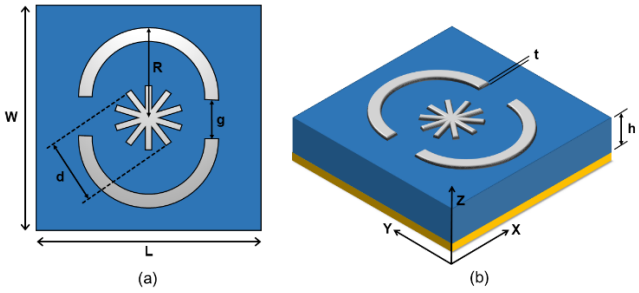

Fig. 1. Schematic of the proposed unit cell absorber (a) top view, and (b) perspective view. The optimised parameters are: $L = 40$ μm, $W = 40$ μm, $R = 18.48$ μm, $g = 10$ μm, $d = 14$ μm, $t = 0.2$ μm, and $h = 9$ μm (color online)

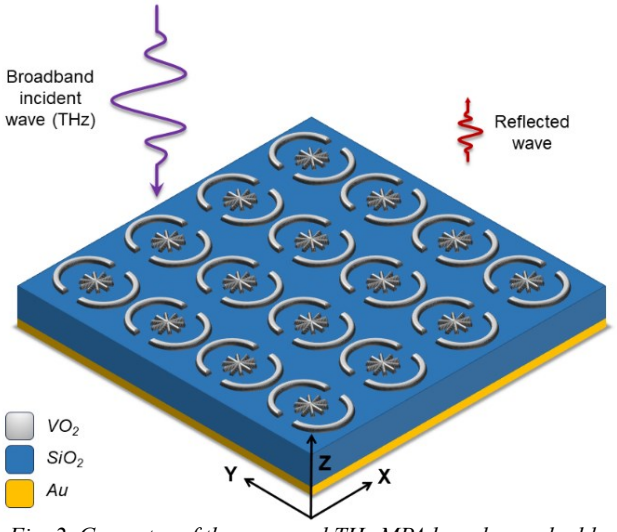

Fig. 2. Geometry of the proposed THz MPA based on a doubly periodic array of VO_2 structures (color online)

2.3. Design evolution

Figs. 3 and 4 depict the evolution stages of the THz perfect absorber design and its corresponding absorption characteristics. Initially, the THz absorber ring-shaped VO_2 resonator synthesized on the SiO_2 plane termed as stage-1, as shown in Fig. 3(a) with outer radius (R) = 18.48 μm. It operates at 4.829 THz and offers 61.01% absorptivity. Further, a plus-shaped resonator is incorporated in stage-1 and termed as stage-2, as described in Fig. 3(b) with a length of each strip, $d = 14$ μm. It achieves 71.06% absorption at 4.759 THz. Now, to improve the absorptivity, more stripes in the plus-shaped resonators are added, as shown in Fig. 3(c), and named stage-3. This improved the absorptivity by 7% and it achieved 78.326% absorption at 4.766 THz. However, these stages are not sufficient to achieve the desired range of absorption. Hence, the ring resonator is split and optimized in such a way that it is resonant at 4.108 THz with an exceedingly high absorptivity of 99.79% (stage-4), as described in Fig. 3(d). The absorber achieves exceptionally high absorption, close to 100%, at a specific terahertz frequency (4.108 THz).

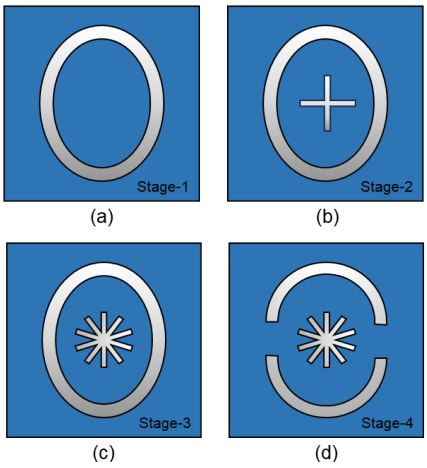

Fig. 3. (a) Stage-1 (b) Stage-2 (c) Stage-3 (d) Stage-4 are the design evolution of the proposed absorber (color online)

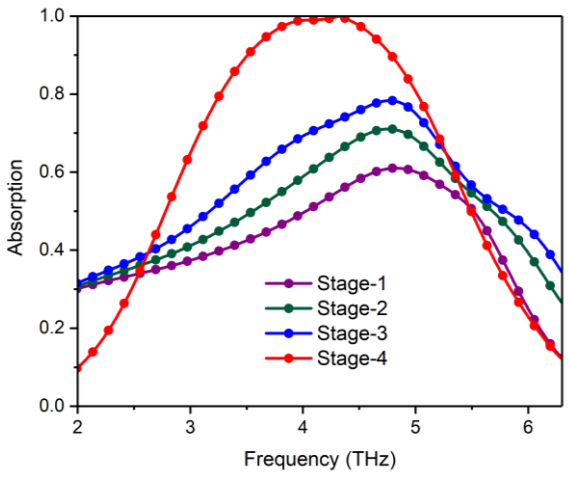

Fig. 4. Absorption characteristics for different stages of the design evolution (color online)

The reflection property is remarkably low, indicating that the incoming THz wave is efficiently absorbed rather than reflected. The figure suggests negligible transmission through the absorber, signifying that the THz wave is almost entirely absorbed within the metamaterial structure. The gold layer positioned beneath the substrate plays a crucial role. It effectively prevents the THz wave from propagating through the backside of the absorber (i.e. $T(\omega) = |S_{12}|^2 = 0$).

2.4. Parametric analysis

a) Effect of substrate thickness on absorption rate

Fig. 5 unveils a relationship between the substrate thickness (h) and the absorption. It demonstrates a critical dependence, where a specific thickness optimizes absorption performance. At h = 9 µm, the absorber achieves an impressive absorption rate of 99.79% at the target resonance frequency of 4.108 THz. This signifies a near-perfect capture of the incoming electromagnetic waves. However, deviating from this ideal thickness leads to a significant decline in absorption efficiency. The graph starkly illustrates this trend. As we increase the substrate thickness to 10 µm, the absorption rate plummets to 83.85%. Further thickening to 11 µm and 12 µm results in even steeper drops, reaching 68.55% and 52.77% absorption, respectively.

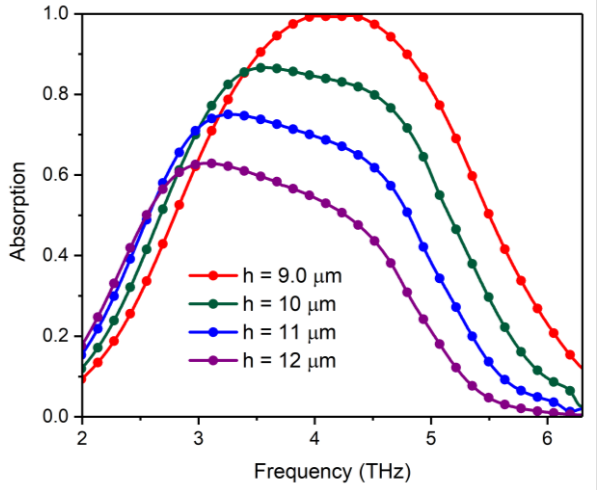

Fig. 5. Absorption characteristics for substrate thickness of the proposed absorber (color online)

b) Effect of length of the star-shaped patch on absorption rate

Analysis of the length of the star-shaped patch shows a significant variation in the absorptivity at the target frequency as depicted in Fig. 6. We can observe that, the length of the star-shaped patch (d) gives the highest absorption rate of 99.79% at d = 14 µm. When we decrease the length of the strip, then there is significant degradation in the absorption rate. From the figure, it is observed that at desired resonant frequency i.e., at 4.108 THz, we get 86.39%, 90.59%, and 95.59% absorptivity when d = 11 µm, d = 12 µm, and d = 13 µm, respectively. For instance, as we vary the length of the star-shaped patch's strip the absorption peak varies significantly.

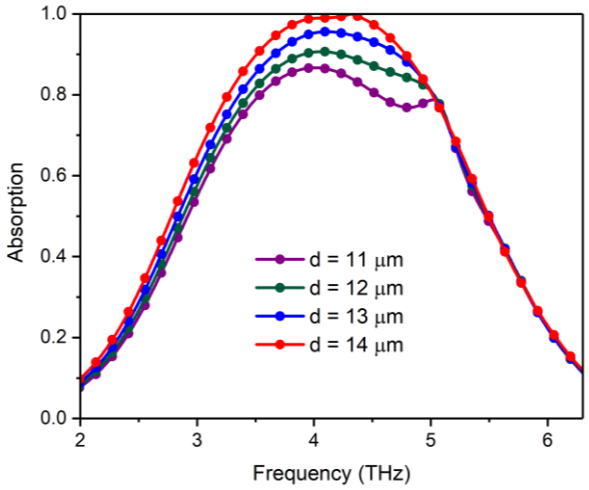

Fig. 6. Absorption characteristics for the length of the star-shaped patch of the proposed absorber (color online)

c) Effect of the size of the split ring patch on absorption rate

Analysis of the size of the split ring patch shows the significant variation in the absorptivity at the target frequency as depicted in Fig. 7. We can observe that the radius of the split ring patch (R) gives the highest absorption rate of 99.79% at R = 18.48 µm. When we decrease the radius of the split ring, then there is a significant degradation in the absorption rate. From the figure, it is observed that at desired resonant frequency i.e., at 4.108 THz, we get 93.23%, 95.34%, and 96.19% absorptivity when R = 18.18 µm, R = 18.28 µm, and R = 18.38 µm, respectively. For instance, as we vary the radius of the split ring patch the bandwidth of the absorber also shows a significant variation.

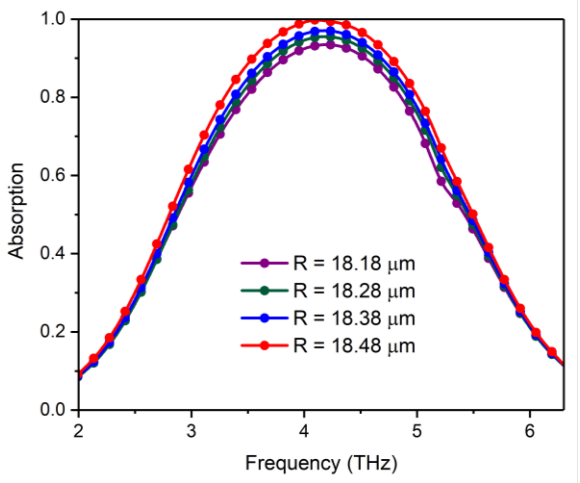

Fig. 7. Absorption characteristics for the size of the split ring patch of the proposed absorber (color online)

3. Results and discussion

Fig. 8 depicts the reflection and absorption spectra of the proposed THz absorber when the VO_2 layer is in its metallic phase with a conductivity of 2×10^5 S/m. The results reveal an impressive absorption bandwidth exceeding 90% ranging from 3.541 THz to 4.773 THz (a bandwidth of 1.232 THz) for normally incident THz waves. The absorber also exhibits a peak absorption at 4.108 THz.

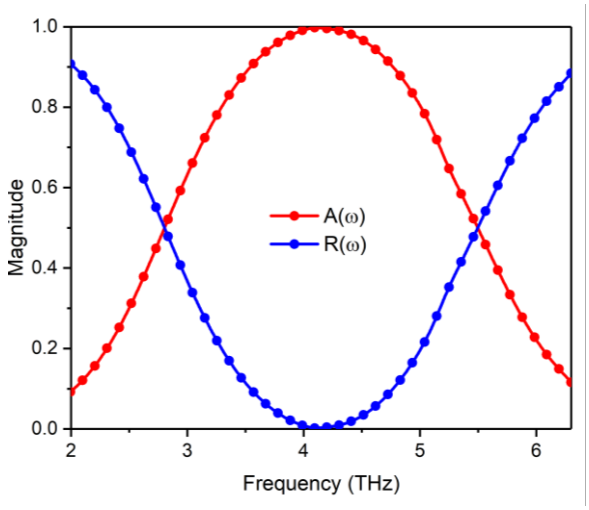

Fig. 8. The reflection and absorption spectrum of the proposed THz absorber (color online)

To gain deeper insights into the absorption mechanism, we employed full-wave simulations using CST Microwave Studio, a commercial software that utilizes the finite-integration technique. The simulations were performed on the proposed unit cell (refer to Fig. 1) under periodic boundary conditions. In the simulations, the SiO_2 layer was modelled as a lossless dielectric with a relative permittivity of 3.8.

To demonstrate the potential for real-world applications, here's a brief overview of possible fabrication steps for the meta-surface. The first step involves depositing a thin silicon SiO_2 film, approximately 9 µm thick, onto a gold substrate using Plasma Enhanced Chemical Vapor Deposition (PECVD). This technique is a well-established method for creating thin films with precise control over thickness and uniformity. Once the VO_x film has been deposited onto SiO_2 film using DC magnetron sputtering with a vanadium metal target, it can be annealed in a low-pressure O_2 atmosphere to yield VO_2 [22]. In the end, VO_2's surface is etched using a photolithography technique to produce the necessary pattern, which is based on the surface pattern's mask. The impedance matching theory also explains the phenomenon of perfect absorption in the absorber as expressed in Eq. (7). This is the source of the effective impedance of the MPA [23].

$$Z = \sqrt{\frac{\mu}{\varepsilon}} = \frac{\sqrt{(1+S_{11})^2 - S_{21}^2}}{\sqrt{(1-S_{11})^2 - S_{21}^2}} \tag{7}$$

where the values for effective permeability (µ) and effective permittivity (ε) are respectively. When the absorber's effective permeability and effective permittivity are equal to free space, as is well known, there won't be any reflection on the surface.

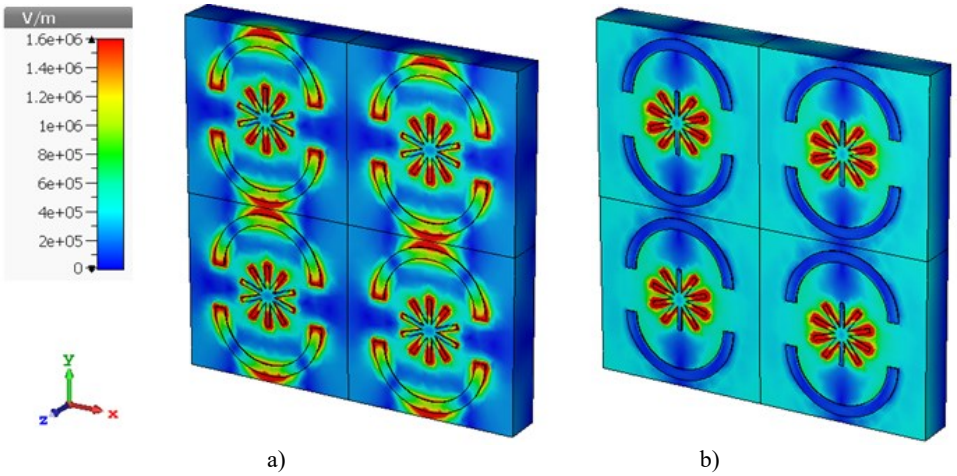

a) b)

Fig. 9. The electric field distribution of the top view at 4.108 THz in (a) horizontal direction and (b) vertical direction (color online)

The absorber's horizontal and vertical electric field distribution at the absorption peak which is 4.108 THz is displayed in Figs. 9(a) and (b), respectively. According to the results shown in the figure. The horizontal electric field at the peak is distributed nearly evenly along the star-shaped patch's strip along with the edges of the split-ring patch, as shown in Fig. 9(a). By comparison in the figure, the verticle electric field at the peak is distributed nearly evenly along the star-shaped patch's strip, as shown in Fig. 9(b).

Multiple resonant structures with different sizes and multi-layer structures with multi-thickness dielectric layers are listed for comparison [24]-[29]. While these structures demonstrate impressive performance, achieving this performance requires complex and challenging fabrication processes. Additionally, precisely controlling key

parameters can be difficult, which may limit their scalability and real-world applicability. The proposed split-ring star-shaped VO_2 metamaterial absorber achieves superior performance compared to previously reported metamaterial perfect absorbers for THz applications as summarized in Table 1. While some reported designs achieve similar bandwidths, our design boasts a significantly higher absorption rate. The proposed design achieves an exceptional absorption of 99.79% at a bandwidth of 1.23 THz. This significantly outperforms the absorption rates reported in Refs. [24] and [27], which achieve lower absorption rates (around 90%) despite having similar or wider bandwidths. Whereas, Refs. [25] and [29] achieve higher absorption rates, their bandwidths are narrower (0.52 THz and 1.25 THz, respectively). Similarly, Refs. [26] and [28] offer wider bandwidths (around 2.4 THz) but with lower absorption rates (around 90%). The proposed design strikes a balance between high absorption and a respectable bandwidth. Moreover, the proposed design utilizes a novel split-ring star-shaped structure, while previous works explored geometries like circles, crosses, rectangular slots, square loops, and *H*-shaped elements. Hence, the split-ring star-shaped VO_2 metamaterial absorber presented in this paper offers a compelling combination of high absorption (99.79%) and a respectable bandwidth (1.27 THz), surpassing the performance of previously reported THz metamaterial absorbers based on the comparison in Table 1. This makes it a highly promising candidate for various THz applications.

Table 1. Comparison of the absorption performance with recent VO_2 based absorbers

Refs.	Absorption Bandwidth	Relative Bandwidth	Shape of the absorber	Absorp-tivity
[24]	0.75 THz	76 %	Circle and cross-shaped patch	90%
[25]	0.52 THz	71 %	Plus-shaped-rectangular slot patch	98%
[26]	2.45 THz	79 %	Square-shaped ring patch	90%
[27]	1.23 THz	25 %	Circular and cross-shaped patch	90%
[28]	0.77 THz	23 %	*H*-shaped dual-element	90%
[29]	1.25 THz	25 %	Square loop and square slot multilayered patch	96%
This Work	1.23 THz	30 %	Split-ring star-shaped patch	99.79%

4. Conclusion

In this work, a split-ring star-shaped VO_2 based MPA is proposed, and its absorbance rates are examined in the THz frequency region. The proposed MPA boasts an impressive absorption rate of 99.79% at a specific THz frequency (4.108 THz). Furthermore, it exhibits a broad THz absorption bandwidth exceeding 90%, ranging from 3.541 THz to 4.773 THz (a bandwidth of 1.232 THz). This wide bandwidth places our design competitively with similar devices reported in the literature. Through meticulous optimization of the geometric structure, we were able to maximize both the absorption bandwidth and efficiency of the MPA. To gain a deeper understanding of the underlying mechanism, we analyzed the electric field distributions within the structure and their influence on absorption properties. This study proposes a remarkably simple design for a MPA achieving exceptional performance in the THz region. The resulting design is not only compact in size but also exhibits near-perfect absorption in the THz range. These characteristics make the proposed MPA a promising candidate for diverse applications, including solar energy harvesting, sensor technology, microbolometers, imaging systems, and even stealth technology.

Author's Contribution

R. A.: concept-original draft, simulation. S. K. G.: Parametric analysis, manuscript writing and figure preparation. A. B.: Supervision of concept, critical analysis, Critical review and Final manuscript preparation.

Funding: There is no funding to declare.

Data Availability: All data and materials are included in the manuscript.

Ethical Approval: This declaration is not applicable**.**

Competing Interests: The authors declare no competing interests.

References

[1] Y. Wen, W. Ma, J. Bailey, G. Matmon, X. Yu, IEEE Trans. Terahertz Sci. Technol. **5**(3), 406 (2015).
[2] X. He, F. Lin, F. Liu, H. Zhang, Nanomaterials **10**(1), 39 (2019).
[3] J. Zhou, Z. Liu, X. Liu, G. Fu, G. Liu, J. Chen, C. Wang, H. Zhang, M. Hong J. Mater. Chem. C **8**(37), 12768 (2020).
[4] L. Chen, Z. Song, Opt. Express **28**(5), 6565 (2020).

[5] C. Yang, Z. Wang, H. Yuan, K. Li, X. Zheng, W. Mu, W. Yuan, Y. Zhang, W. Shen, IEEE Photonics J. **11**(4), 1 (2019).
[6] Z. Song, J. Zhang, Opt. Express **28**(8), 12487 (2020).
[7] H. Wang, V. P. Sivan, A. Mitchell, G. Rosengarten, P. Phelan, L. Wang, Sol. Energy Mater. Sol. Cells **137**, 235 (2015).
[8] A. E. Culhaoglu, A. V. Osipov, P. Russer, IEEE Trans. Antennas Propag. **61**(1), 462 (2012).
[9] S. Guddala, R. Kumar, S. A. Ramakrishna, Appl. Phys. Lett. **106** (11), 111901 (2015).
[10] N. I. Landy, S. Sajuyigbe, J. J. Mock, D. R. Smith, W. J. Padilla, Phys. Rev. Lett. **100**(20), 207402 (2008).
[11] L. Cong, S. Tan, R. Yahiaoui, F. Yan, W. Zhang, R. Singh, Appl. Phys. Lett. **106**(3), 031107 (2015).
[12] H. Deng, L. Stan, D. A. Czaplewski, J. Gao, X. Yang, Opt. Express **25**(23), 28295 (2017).
[13] M. Jiang, Z. Song, Q. H. Liu, Opt. Commun. **471**, 125835 (2020).
[14] G. Wu, X. Jiao, Y. Wang, Z. Zhao, Y. Wang, J. Liu, Opt. Express **29**(2), 2703 (2021).
[15] D. Smith, E. Shiles, M. Inokuti, E. Palik, Handb. Opt. Constants Solids **1**, 369 (1997).
[16] Z. Li, Y. Wang, J. Xiao, Theor. Appl. Mech. Lett. **6**(1), 11 (2016).
[17] P. Rufangura, C. Sabah, Vacuum **120**, 68 (2015).
[18] Y. Zhu, Y. Zhao, M. Holtz, Z. Fan, A. A. Bernussi, J. Opt. Soc. Am. B **29**(9), 2373 (2012).
[19] M. Liu, H. Y. Hwang, H. Tao, A. C. Strikwerda, K. Fan, G. R. Keiser, A. J. Sternbach, K. G. West, S. Kittiwatanakul, J. Lu, S. A. Wolf, F. G. Omenetto, X. Zhang, K. A. Nelson, R. D. Averitt, Nature **487**(7407), 345 (2012).
[20] J. Hao, J. Wang, X. Liu, W. J. Padilla, L. Zhou, M. Qiu, Appl. Phys. Lett. **96**(25), 251104 (2010).
[21] Y. Lou, D. Wu, Y. Pang, Adv. Fiber Mater. **1**, 83 (2019).
[22] L. Xiao, H. Ma, J. Liu, W. Zhao, Y. Jia, Q. Zhao, K. Liu, Y. Wu, Y. Wei, S. Fan, K. Jiang, Nano Lett. **15**(12), 8365 (2015).
[23] D. R. Smith, S. Schultz, P. Markoš, C. M. Soukoulis, Phys. Rev. B **65**(19), 195104 (2002).
[24] S. Wang, C. Cai, M. You, F. Liu, M. Wu, S. Li, H. Bao, L. Kang, D. H. Werner, Opt. Express **27**(14), 19436 (2019).
[25] Z. Song, M. Wei, Z. Wang, G. Cai, Y. Liu, Y. Zhou, IEEE Photonics J. **11**(2), 1 (2019).
[26] J. Bai, S. Zhang, F. Fan, S. Wang, X. Sun, Y. Miao, S. Chang, Opt. Commun. **452**, 292 (2019).
[27] R. Dao, X. Kong, H. Zhang, X. Su, Optik **180**, 619 (2019).
[28] J. Huang, J. Li, Y. Yang, J. Li, J. li, Y. Zhang, J. Yao, Opt. Express **28**(5), 7018 (2020).
[29] J. Huang, J. Li, Y. Yang, J. Li, J. Li, Y. Zhang, J. Yao, Opt. Express **28**(12), 17832 (2020).

*Corresponding author: abage@nith.ac.in